Instability Regions in the Upper HR Diagram

Cornelis de Jager*
SRON Laboratory for Space Research
Sorbonnelaan 2, 3584 CA Utrecht, NL

Alex Lobel
Harvard-Smithsonian Center for Astrophysics
60 Garden Street, Cambridge, MA 02138, USA

Hans Nieuwenhuijzen
SRON Laboratory for Space Research
Sorbonnelaan 2, 3584 CA Utrecht, NL

Richard Stothers
Goddard Institute for Space Studies, NASA
2880 Broadway, New York, NY 10025, USA

10 March 2001

Abstract

The following instability regions for blueward evolving supergiants are outlined and compared: (1) Areas in the Hertzsprung-Russell (HR) diagram where stars are dynamically unstable. (2) Areas where the effective acceleration in the upper part of the photospheres is negative, hence directed outward. (3) Areas where the sonic points of the stellar wind (where $v_{wind} = v_{sound}$) are situated inside the photospheres, at a level deeper than $\tau_{Ross} = 0.01$. We compare the results with the positions of actual stars in the HR diagram and we find evidence that the recent strong contraction of the yellow hypergiant HR8752 was initiated in a period during which $< g_{eff} > < 0$, whereupon the star became dynamically unstable. The instability and extreme shells around IRC+10420 are suggested to be related to three factors: $< g_{eff} > < 0$; the sonic point is situated inside the photosphere; and the star is dynamically unstable.

Key words: stars: atmospheres; interiors; supergiants; evolution; HR-diagram

*email: C.dejager@sron.nl

1 Introduction; hypergiant instability

The apparent instability of many stars in the upper part of the HR diagram has different causes, dependent on the stellar properties, which, in turn, are partly related to their locations in the HR diagram. Observations obtained in recent years are indicative of various modes of interior or atmospheric instabilities among yellow hypergiants and S Dor stars (=LBV's). Evidences for these instabilities in yellow hypergiants were summarized by de Jager (1998). Specifically, they refer to phenomena such as the enormous pulsational amplitude ($\Delta R \simeq 0.25R$) of ρ Cas (Lobel et al., 1997), the 'bouncing' evolutionary motions of ρ Cas (reviewed by de Jager, 1998), of IRC+10420 (Oudmaijer et al., 1994), of Var A in M33(Humphreys, 1975, 1978) and of HR8752 (de Jager and Nieuwenhuijzen, 1997). Another indication of atmospheric instability may be seen in the extended clouds of gas and dust around IRC+10420 (Mutel et al., 1979; Jones et al., 1993; Oudmaijer et al., 1996; Blöcker et al., 1999). In S Dor stars the large outbursts and the quasi-oscillatory temperature changes (*cf.* review by van Genderen, 2001) have been suggested to be due to their dynamic instability (Stothers and Chin, 1996). The understanding of the causes of these instabilities may profit from a delineation of areas where one or the other mode of instability prevails. It should be noted in this connection that, when speaking of stellar instability, we do not refer to the observed microvariations (reviewed by van Genderen, 2001) whose origin might possibly be sought in the excitation of strange mode pulsations or other low-amplitude radial or non-radial oscillations.

We summarise earlier work in this field.

Stothers and Chin (1996) showed that in certain areas of the HR diagram the mean value of $\Gamma_1 (= (\mathrm{d}\ln P/\mathrm{d}\ln\rho)_{ad})$ can take values below 4/3, which implies dynamic instability of the star. As a consequence, a highly evolved star to which this applies can be triggered to a phase of steady expansion or contraction. Thus, they were able to define two regions of dynamic instability in the upper part of the HR diagram, one for $T_{eff} \leq 10000$, another for higher temperatures. These areas were called the 'yellow-red' and the 'blue' dynamic instability regions.

Nieuwenhuijzen and de Jager(1995, summarized by de Jager, 1998) outlined two regions in the HR diagram where in the atmospheres of blueward evolving stars, hence very evolved objects, five conditions are obeyed. These are: $g_{eff} < 0.3\ \mathrm{cm\,s^{-2}}$; $\mathrm{d}\rho/\mathrm{d}z < 0$ (z is the vertical ordinate) in the relatively deep parts of the photospheres; the sonic point, *i.e.* the level where $v_{wind} = v_{sound}$, lies inside the photosphere; the sum $g_{eff} + g_{puls} < 0$ during part of the pulsation; and $\Gamma_1 < 4/3$ in part of the line-forming part of the photosphere. Their two regions were baptised the 'yellow void' and the 'blue instability region'.

In our studies of supergiant instabilities it became clear to us that it may advance the understanding of stellar instability (or quasi-instability) by considering the various causes *separately*. To that end we will delineate the regions in the HR diagram where supergiants or their atmospheres are unstable in one

way or the other.

2 Areas of stellar dynamic instability

Ritter (1879) showed that for radial dynamic stability the ratio of specific heats γ should exceed the value 4/3. More generally, Ledoux (1958) found that for a real star the first generalised adiabatic exponent Γ_1, suitably averaged, should exceed 4/3 in order that the star be dynamically stable. Following that line, Stothers and Chin (1995) and Stothers (1999) demonstrated that a non-adiabatic, spherically symmetric envelope of a star is dynamically unstable when $\sigma^2 \leq 0$, where σ^2 is the square of the adiabatic eigenfrequency. Here:

$$\sigma^2 = \frac{(3 < \Gamma_1 > -4) \int_r^R P \, \mathrm{d}(r^3)}{\frac{1}{3} \int_r^R r^2 \rho \mathrm{d}(r^3)}, \tag{1}$$

with

$$< \Gamma_1 >= \frac{\int_r^R \Gamma_1 \; P \, \mathrm{d}(r^3)}{\int_r^R P \, \mathrm{d}(r^3)}. \tag{2}$$

The lower bound r of the integration was placed at the bottom of the outer envelope, which is in all his cases deep inside the star, mostly very close in distance to the centre. Formally, it should be placed at the very centre, at $r = 0$, but truncation to a small r-value is allowed because at the base of the envelope the relative amplitude $\Delta r/r$ is already many powers of ten smaller than its value at the surface and therefore the deepest regions do not contribute to the stellar (in)stability.

Stothers (1999) gave various examples of the behaviour of stellar models for different values of $< \Gamma_1 >$. We quote one of them: his Fig. 2 shows the time-dependent distance from the stellar centre of various layers of a dynamically unstable and pulsationally stable supergiant ($\log L/L_\odot = 6$; $T_{eff} = 10\,000$). In that case a value $< \Gamma_1 > = 1.330$ was found, which implies, with eq. (1), a negative value of σ^2. Hence, the model should be dynamically unstable, and this is confirmed by the model calculations. An additional result is that the model appears to be pulsationally stable.

Two comments are here in order. First, it appears, from a look at the model calculations given, that stars where $< \Gamma_1 > <$ or $> 4/3$ are often also (but in rough approximation only) pulsationally unstable or stable, respectively. Next, one may wonder whether averaging Γ_1 over the *atmosphere only* can also give information on the instability of the whole star, because for the stars situated in the upper part of the HR diagram the atmosphere occupies a considerable fraction of the star. We refer to our Fig. 4 which shows that $\Delta r/R$ (where Δr is the depth range between $\tau_R = 0.001$ and 10) attains values of the order of 0.1 to more than 0.3. A comparison with Stothers's model calculations shows

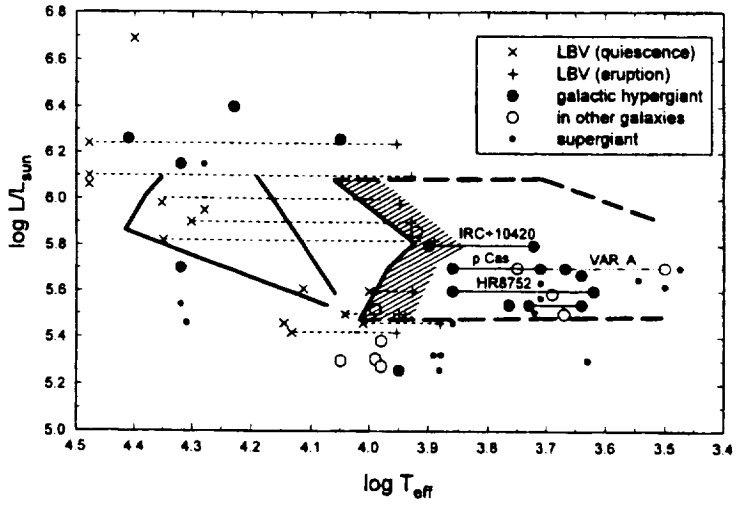

Figure 1: Areas in the upper part of the HR diagram where stars are dynamically unstable according to the criterion $< \Gamma_1 > < 4/3$.The diagram shows the 'yellow-red' and the 'blue' dynamic instability regions. No model calculations are so far available above and below the upper and lower dashed horizontal lines, respectively.

that this extent is not large enough, because $\Delta r/R$ is still considerable at $\tau_R = 10$.

The question that is relevant to the present study is that of the delineation of the areas in the HR diagram where $< \Gamma_1 > < 4/3$. The data for the yellow-red hypergiant region are given in Fig. 2 of Stothers and Chin (2001). In that paper, particular attention was given to the high-temperature border line. Its position, depending on the assumed value for the parameter for convective mixing, is given in our Fig. 1. The positions of the lower and upper boundary of the yellow-red instability area are tentative.

The definition of the blue area is more uncertain. It can be read from Stothers and Chin (1996), where the instability area, for a metal ratio Z = 0.03, is displayed in their Figs. 1 and 2. The red edge parameters are listed in Table 1 of the quoted paper. The blue area has a high-luminosity cut-off around $\log(L/L_\odot) = 6.1$. This value is uncertain; it may be as low as 5.9. The low-luminosity cut-off is around $\log(L/L_\odot) = 5.4$. The tentative border lines of the blue area are also drawn in our Figure 1.

Two aspects are brought forward by Figure 1: the yellow-red area contains all red and yellow hypergiants. The blue area contains virtually all S Dor stars (= LBV's) in their stable states. This is one of the bases for the assumption (Stothers and Chin, 2001, in line with Lamers et al., 1983) that yellow hyper-

giants are dynamically unstable stars that are evolving blueward and that, having entered the blue instability region, show up as S Dor stars (LBV's). This assumption implies that S Dor stars are very evolved, dynamically unstable, stars.

3 Photospheric instability defined by $g_{eff} < 0$; the case of HR8752

In order to study photospheric instability we have calculated photospheric models and derived from these models the four components of the acceleration: the Newtonian acceleration, g_N; the radiative value, g_r; the turbulent acceleration, g_t; and the acceleration due to the wind, g_w. They add up to g_{eff}. For stars with T_{eff} below to roughly around 10 000 K, the turbulent and Newtonian components are the most important ones; for hotter stars g_r contributes too, and for the hottest and most luminous ones g_w becomes a major component. Cases can occur in which their sum, g_{eff}, is negative, hence directed outward. For cool stars, g_N and g_t are the competing components. Actually, for the most luminous cool objects the absolute value of g_t can exceed that of g_N, and in that case g_{eff} will be directed outward. We refer to Table 1, further below.

For the computations, the input parameters of the models are, apart from $L/L_\odot$ and T_{eff}:

- The stellar mass, $M/M_\odot$. This value is derived from Maeder and Meynet (1988). We took their masses for blueward evolving stars. An interpolation programme was developed to obtain $M/M_\odot$ for input $L/L_\odot$ and T_{eff} values.

- The stellar rate of mass loss, $\dot{M}$. These values were taken from de Jager, Nieuwenhuijzen and van der Hucht (1988). We realise that some authors advocate the use of higher values of $\dot{M}$ for the most luminous stars (factors 2 and even 3 are sometimes mentioned) but we decided to stick to the published data for the sake of consistency and also because there are no compelling observational reasons yet that suggest higher $\dot{M}$ values. Anyway, the value of g_w, which depends on $\dot{M}$, is in no case a decisive contributor to g_{eff}.

- The microturbulent velocity component in the line-of-sight, ζ_μ. This quantity is unknown over the greater part of the HR diagram. Since input data are needed for a consistent photospheric model, we had a look at the literature and compared the observationally derived ζ_μ values with the photospheric sound velocity v_s at $\tau_R = 0.67$. We found for the ratio ζ_μ/v_s values ranging between 1.4 and 2.2, and clustering around 2. Therefore we decided to make the computations for two cases: $\zeta_\mu = v_s$ (in order to have a 'minimum case') and $\zeta_\mu = 2v_s$, which may be more than a maximum case for the most luminous hot stars, because for such stars, for which the sonic point is situated in photospheric regions (Fig. 3), the large observed ζ_μ-value is partly due to the strong $v(\tau)$ gradient over the region of line formation, and the real value of ζ_μ

is therefore smaller. An example is the B2 supergiant HR80077 (Carpay et al., 1989) for which $\zeta_\mu = 23\,\mathrm{km\,s^{-1}}$. For cooler and less luminous stars $\zeta_\mu = 2v_s$ is a valid approximation.

The various accelerations were derived on the basis of the equation of conservation of momentum, written as

$$\frac{-\mathrm{d}P_g}{\rho \mathrm{d}z} = \frac{GM}{r^2} + g_r(r) + \frac{\mathrm{d}(v_w)^2}{2\mathrm{d}z} + \frac{(\zeta_\mu)^2 \mathrm{d}\ln\rho}{2\mathrm{d}z}, \tag{3}$$

in which we write

$$g_r = \frac{1}{\rho}\frac{\mathrm{d}P_r}{\mathrm{d}z}, \tag{4}$$

where

$$P_r = \frac{1}{c}\int I_\omega \cos^2\theta \mathrm{d}\omega. \tag{5}$$

Further

$$v_w = \frac{-\dot{M}}{4\pi r^2 \rho}. \tag{6}$$

Eq. (3) is written as

$$g_{eff} = g_N + g_r + g_w + g_t. \tag{7}$$

which defines the four components and their sum. All five quantities are depth dependent, and not to a small degree: Cases are rare in which g_{eff} varies by less than a factor 2 over the photosphere and there are many cases in which the range is larger than a factor 10. Evidently, the structure of a photosphere in which g_{eff} varies over such a large range differs greatly from one in which it is constant with depth.

To illustrate the relative importance of the g-components for various combinations of T_{eff} and $L/L_\odot$, we refer to Table 1.

In view of the strong variability of $g_{eff}(\tau)$ the photospheric models were derived by an iterative method. With the above input values and with an estimated initial value for g_{eff} (we took $(g_{eff})_{in} = g_N + g_r$ at $\tau = 0.67$) a photospheric model was interpolated in the Kurucz set of models. For that model the depth dependent values of g_{eff} were calculated.

The next step was a calculation of a model with these depth-dependent $g_{eff}(\tau)$ values, on the basis of a $T(\tau)$ relation interpolated in the Kurucz models for the given value of T_{eff} and the average g_{eff} value. For the new model $g_{eff}(\tau)$ was derived anew and a new (third approximation) model with depth-dependent $g_{eff}(\tau)$ was derived; a process that was repeated until convergence was reached, in the sense that the new $< g_{eff}(\tau) >$ did not differ significantly from that of the previous step.

Table 1: The components of g_{eff} at an optical depth of $\tau_R = 0.1$ in photospheres defined by some combinations of T_{eff} and $\log(L/L_\odot)$; the latter written in the table heading as L. The table also gives the corresponding stellar mass $M/M_\odot$ (written in the heading as M) for blueward evolution, the corresponding rate of mass loss $-\log\dot{M}$ (written as $\dot{M}$), and the assumed microturbulent velocity component ζ_μ. M, $\dot{M}$ and ζ_μ were derived as described in the text. The microturbulence is in $\mathrm{km\,s^{-1}}$ and the accelerations in $\mathrm{cm\,s^{-2}}$.

T_{eff}	L	M	$\dot{M}$	ζ_μ	g_N	g_r	g_t	g_w	g_{eff}
7079	5.45	7.91	4.86	4.94	1.68	-.02	-.32	0	1.34
7079	6.05	34.60	3.32	4.81	1.87	-.02	-.37	0	1.48
7943	5.35	7.50	5.17	15.25	2.55	-.13	-.78	0.01	1.65
7943	5.7	13.1	4.47	7.48	2.31	-.12	-.54	0.01	1.66
10000	6.0	32.7	4.94	20.11	7.55	-.76	-4.80	0.05	2.04
15850	5.7	19.8	5.24	13.80	35.0	-3.6	-.7	1.3	32.0

Table 2: A typical course of the iterations for a model with low T_{eff}. Here, τ_{son} is the optical depth of the sonic point, $< g_{eff} >$ is the average value of g_{eff} over the τ_R interval between 0.007 and 0.75, and $< g_{eff} >_{out}$ is the average over the depth region 0.007 to 0.2. The model is for $T_{eff} = 7079$ K and $\log(L/L_\odot) = 5.9$; $\zeta_\mu = 4.87$ km s^{-1}.

iteration #	τ_{son}	$< g_{eff} >$	$< g_{eff} >_{out}$
1	-	0.79	0.79
2	.0017	1.55	1.46
3	.0007	1.44	1.29
4	.0007	1.47	1.34
5	.0007	1.46	1.33

Table 3: As Table 2, but for a higher temperature. T_{eff} = 15850 K and $\log(L/L_\odot) = 5.7$; $\zeta_\mu = 13.8$ km s^{-1}.

iteration #	τ_{son}	$< g_{eff}$	$< g_{eff} >_{out}$
1	-	90	90
2	.29	56	53
3	.004	22	11
4	.11	34	22
5	.012	48	42
6	.007	38	29
7	.012	49	44
8	.007	36	28

For low values of T_{eff}, roughly for $T_{eff} < 10000$ K, convergence was normally reached in 3 to 4 iterations, as is shown in the example of Table 2. As a rule we stopped after the fourth or fifth iteration. For higher temperatures, where all four g-components come into play, successive iterations appear to alternate around an average value, as is shown in the example of Table 3. We checked that this average is close to the 'best' value and therefore, starting with the fourth iteration, we usually took as input parameters for the 2nth iteration the average values of $g_{eff}(\tau)$ between those of the $(2n-1)$th and the $(2n-2)$th iterations. This procedure worked well.

For the resulting model two values for the average of g_{eff} were derived. The first, called $< g_{eff} >$, is the average over the depth interval $\tau = 0.007$ to 0.75; the other, $< g_{eff} >_{out}$ was averaged over a more outer region: 0.007 to 0.2. There are models for which the latter is negative while the former is not. These models thus define a transition region between models for which the average g_{eff} values are positive and negative respectively. That transition region is too thin to make it well visible in Fig. 2.

Note in Fig. 2 the position of the region with $< g_{eff} > < 0$. It strikes us that the three stars mentioned earlier (ρ Cas, HR8752 and IRC+10420) are all situated close to the line $< g_{eff} > = 0$. IRC+10420 even lies in the region of negative values. This suggests that the low-temperature border line of the area where $< g_{eff} > \leq 0$ is an obstacle for blueward moving supergiants. This observation implies that the hypergiant characteristics are (at least partly) related to their positions in and near that instability area. Earlier, two of us (de Jager and Nieuwenhuijzen, 1997) described the repeated to-and-fro movemements of HR8752 along the T_{eff} axis as 'bouncing against the border of the instability region'. Fig. 2 specifies the location of the bouncing as the low-T_{eff} border of the area where $g_{eff} < 0$. The object HR8752 is remarkable in that respect. Starting around the years 1983 - 1985, its T_{eff} value has steadily and dramatically increased till about the year 1998 (Israelian et., 1999), which implies a steady compression, reminiscent of a dynamic instability (Nieuwenhuijzen and

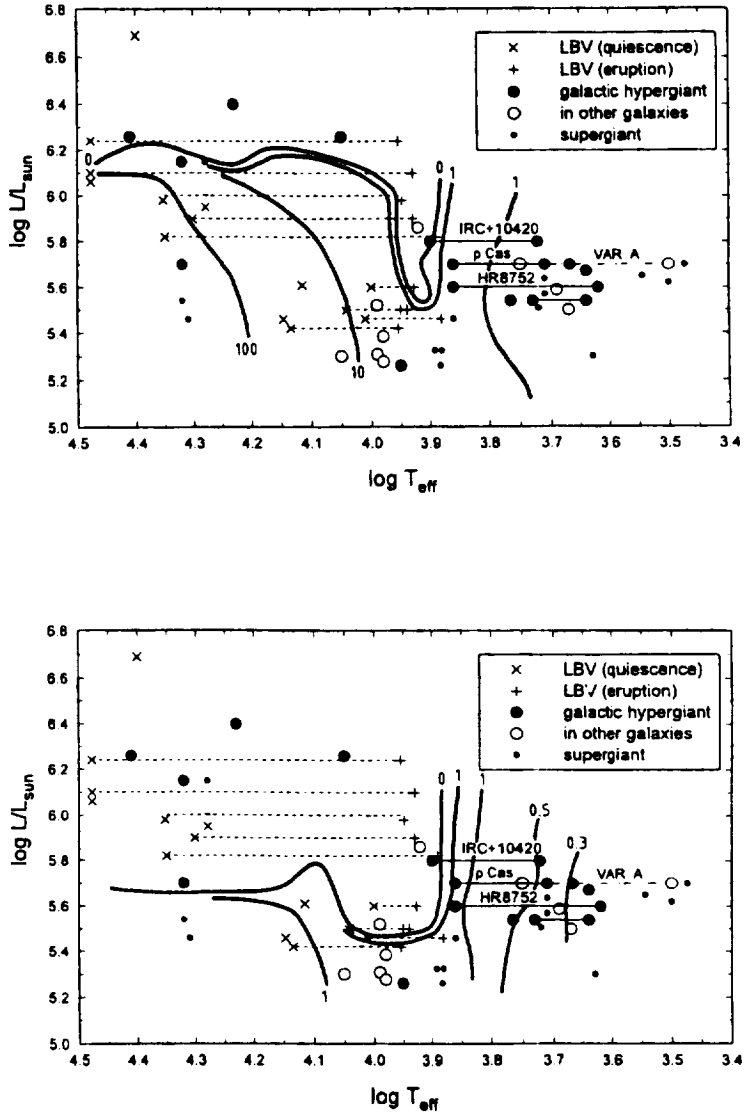

Figure 2: The HR diagram with lines of equal $< g_{eff} >$ values. The upper diagram is for $\zeta_\mu = v_s$; the other is for twice these values.

de Jager, 2000; de Jager et al., 2001). We think that this behaviour can be interpreted as a dynamic instability triggered by the decrease of $< g_{eff} >$ to below zero. The observations show that $< g_{eff} > \ < 0$ the last time in 1978. That period was followed by one of enhanced mass loss (around 1980 - 1982), and that event was followed, starting in the period 1983 - 1985, by the long period of T_{eff} increase.

4 The depth of the sonic point

Along the lines described in the previous section we derived the optical depth τ_{son} where the wind velocity equals that of sound. Fig. 3 gives lines in the HR diagram of constant τ_{son} values, again for the two assumed values for ζ_μ. We draw attention to the position of IRC+10420 and the neighbouring hypergiant HD33579 (open circle in the diagrams). The latter star cannot be used to check the results of Fig. 3, because it is a redwards evolving star, as follows from its chemical abundances (Humphreys et al., 1991), and from its large mass (Nieuwenhuijzen and de Jager, 2000). The other object though, IRC+10420, is an evolved post-red star (Klochkova et al., 1997, Blöcker et al, 1999; Nieuwenhuijzen and de Jager, 2000). It is rapidly evolving blueward, though not as quickly as HR8752: its spectral type changed from F8 I^+ in 1973 to mid-A in 1998. Hence its effective temperature has increased by about 2000 K in these 26 years. We forward the hypothesis that its instability is due to the combination of three causes: The star is located at the boundary of the $< g_{eff} > < 0$ area and inside the $\tau_{son} > 0.01$ area, and the object is also dynamically unstable (cf. Fig. 1). These effects may explain the instability and the large surrounding gas clouds. Blöcker et al. (1999) suggest that a phase of heavy mass loss occurred some 60 to 90 years ago.

One aspect of the large τ_{son} values is that the replacement time t_{repl} of the photosphere is relatively short. We estimate it at H/v_s where H is the scale height. Inserting the expressions for the two variables and taking μ and γ equal to unity (for order-of-magnitude considerations), one obtains $t_{repl} = (\Re T_{eff})^{1/2}/g_{eff}$. For a star with $T_{eff} = 10\,000$ K and $g_{eff} = 1$ we have $t_{repl} = 10$ days.

A related matter is that of the relative extent of the photospheres. To get an impression, we calculated for a number of the model atmospheres the value of $\Delta r/R$, where r is the radial distance between the levels with $\tau_R = 0.001$ and 10. The outcome is presented in Fig. 4. It appears that for the three unstable yellow hypergiants that were mentioned several times in this paper the relative extent of the photosphere is larger than 0.3, a considerable fraction of the star.

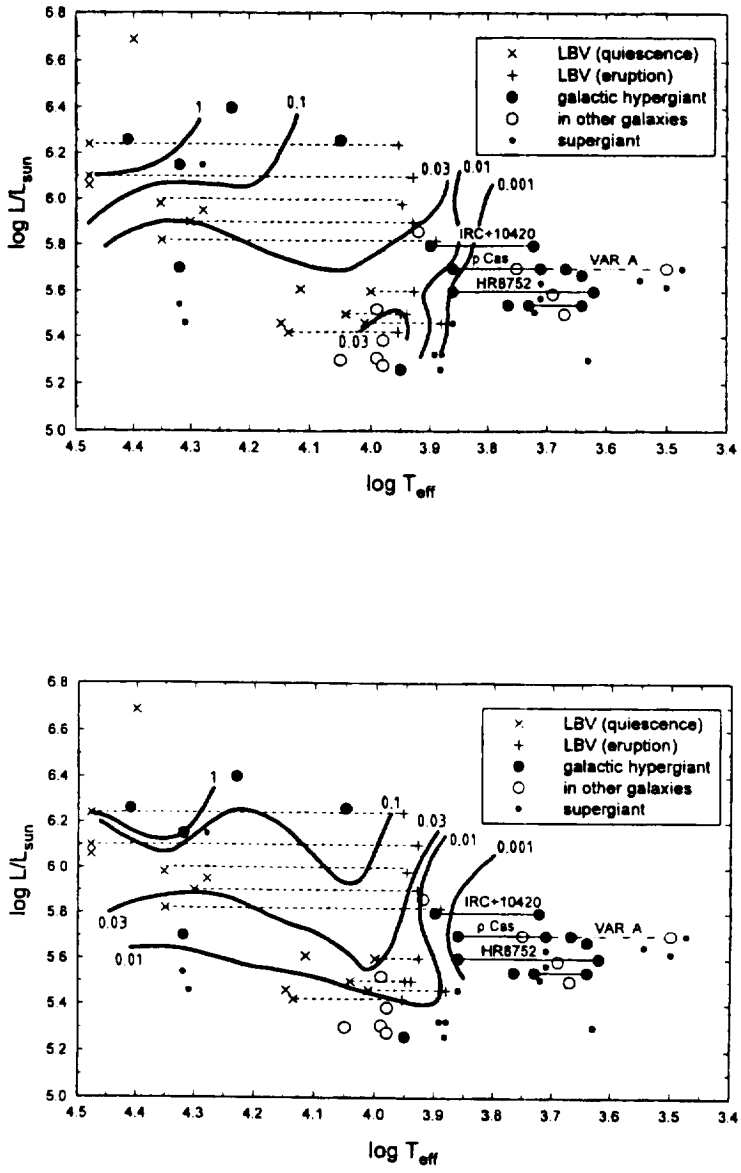

Figure 3: The HR diagram with lines of equal τ_{son} values. The upper diagram is for $\zeta_\mu = v_s$ at $\tau_R = .67$. The lower one is for twice these values.

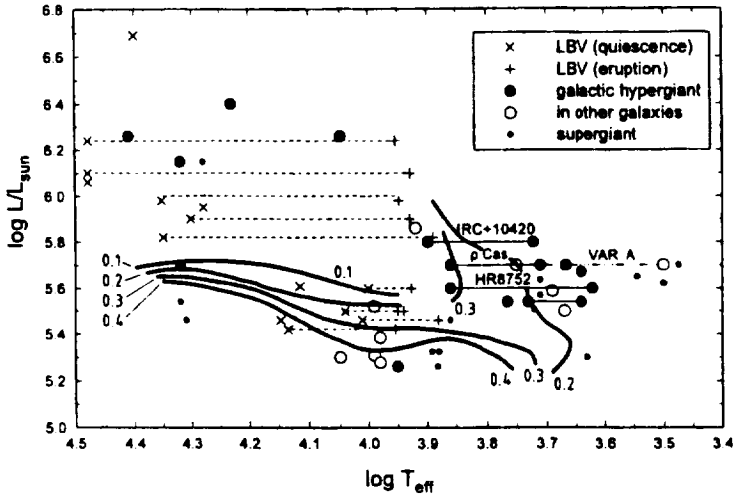

Figure 4: Lines of equal $\Delta r/R$-values in the upper HR diagram. Δr is the radial distance between the levels with $\tau_R = 0.001$ and 10; R is the stellar radius. The diagram is for the case $\zeta_\mu = 2v_s$.

5 Conclusions

The main results of this study are contained in Figs. 1 to 3. They demonstrate the presence of two regions of stellar interior dynamic instability, one in the yellow-red and another in the blue part of the HR diagram. In addition, it appears that the atmospheres of blueward evolving supergiants become unstable when their effective temperature has risen to about 8000 K, for two reasons: The average g_{eff} value becomes negative, and the sonic point is getting situated in photospheric regions.

We have compared these results with the recent life histories of two yellow hypergiants, HR8752 and IRC+10420, and we have shown that their behaviour can be explained on the basis of the data presented in this paper.

It is obvious that the two areas in the HR diagram, defined by $g_{eff} < 0$ and by $\tau_{son} > 0.01$ differ in shape and position from the 'yellow void' and the 'blue instability region', as described in section 1. That is because these latter two regions were defined according to five criteria. We think that the present study does not invaliditate the earlier results, but they do allow more specific studies of atmopsheric instability.

References

[] Blöcker T., Balega Y., Hofmann K.-H., Lichtenthäler J., Osterbart R., Weigelt G.: 1999, A&A 348, 805

[] Carpay J., de Jager C., Nieuwenhuijzen H., Moffat A.: 1989, A&A 216, 143

[] de Jager C., Nieuwenhuijzen H.: 1997, MNRAS 290, L50

[] de Jager C.: 1998, A&A Rev. 8, 145

[] de Jager C., Lobel A., Israelian G., Nieuwenhuijzen H.: 2001, in M. de Groot (ed.) *Armagh P Cyg Workshop*, ASP Conf. Series, in press

[] Humphreys R.M.: 1975, ApJ 200, 426

[] Humphreys R.M.: 1978, ApJ 219, 445

[] Humphreys R.M., Kudritzki R.P., Groth H.G.: 1991, A&A 245, 593

[] Israelian, G., Lobel, A. and Schmidt, M.: 1999, ApJ 523, L145

[] Jones T.J., Humphreys R.M., Gehrtz R.D., Lawrence G.F., Zickgraf F.J., Moseley H., Casey S., Glaccum W., Koch C.J., Pina R., Jones B., Venn K., Stahl O., Starrfield S.G.: 1993, ApJ 411, 323

[] Klochkova V.G., Chentsov E.L., Panchuk V.E.: 1997. MNRAS 292, 19

[] Lamers H.J.G.L.M., de Groot M., Cassatella A.: 1983, A&A 123, L8

[] Ledoux P.: 1958, in S. Flügge (ed.) *Handbuch d. Physik* 51, 605

[] Lobel A., Israelian G., de Jager C., Musaev F., Parker J.Wm., Mavrogiorgou A.: 1998, A&A 330, 659

[] Maeder A., Meynet G.: 1988, A&A Suppl. 76, 411

[] Mutel R.L., Fix J.D., Benson J.M., Webber J.C.: 1979, ApJ 228, 771

[] Nieuwenhuijzen H., de Jager C.: 1995, A&A 302, 811

[] Nieuwenhuijzen H., de Jager C.: 2000, A&A 353, 163

[] Oudmaijer R.D., Geballe T.R., Waters L.B.F.M., Sahu K.C.: 1994, A&A 281, L33

[] Oudmaijer R.D., Groenewegen M.A.T., Matthews H.E., Blommaert J.A.D.L., Sahu K.C.: 1996, MNRAS 280, 1062

[] Ritter A.: 1879, Wiedemann's Annalen der Physik u. Chemie 8, 157

[] Stothers R., Chin C.-w.: 1996, ApJ 468, 842

[] Stothers R.: 1999, MNRAS 305, 365

[] Stothers R., Chin C.-w.: 2001, *Yellow Hypergiants as dynamically unstable post-red supergiant stars*, MNRAS, submitted

[] van Genderen A.M.: 2001, A&A 366, 508